scientific reports

Check for updates

OPEN

Beam steerable MIMO antenna based on conformal passive reflective metasurface for 5G millimeter wave applications

Bilal Tariq Malik[1], Shahid Khan[1] & Slawomir Koziel[1,2]✉

A conformal reflective metasurface fed by a dual-band multiple-input multiple-output (MIMO) antenna is proposed for low-cost beam steering applications in 5G Millimeter-wave frequency bands. The beam steering is accomplished by selecting a specific port of MIMO antenna. Each MIMO port is associated with a beam that points in a different direction due to a conformal reflective metasurface. This novel conformal metasurface antenna design has the advantages of higher gain, lower cost, a simpler feeding source, and a lower profile when compared to traditional reflective metasurfaces using bulky horn antennas and phased arrays with complex feeding networks and phase shifters for beam steering. The proposed beam steering antenna consists of a compact five-element dual-band MIMO and a 32×32 unit-cell conformal dual-band reflective metasurface placed at the top of the MIMO antenna to obtain the beam steering capability as well as gain enhancement. The proposed reflective metasurface has a stable response under oblique incidence angles of up to 60^0 at 24 GHz and 38 GHz and its symmetric, single-layer structure, ensures polarization insensitivity and stable response under conformal conditions. The presented MIMO antenna design is not only compact but also offers a wideband response effectively covering the desired 5G mm-wave frequency bands. The overall size of the MIMO antenna alone is 70 $\times$ 12 mm^2 with a maximum gain of 5.4 and 7.2 dB. It is further improved up to 13.1 and 14.2 dB at 24 and 38 GHz respectively, with a beam steering range of ś40^0 by using a conformal reflective metasurface. Unlike the existing beam steering strategies, the suggested method is not only cost-effective but also increases the overall directivity and gain of the source MIMO antenna. The measured results agree with the simulated results, making it a potential candidate in the 5G and beyond beam steering applications.

Keywords Beam steering, Metasurface, Millimeter wave, MIMO, 5G

The millimeter-wave (mm-wave) frequency range is promising for achieving ultra-fast connectivity. However, the mm-wave signal is blocked and attenuated by buildings or objects. In real life, we need cost-effective, high-gain beam-steering antennas that can send and receive signals in different directions to compensate for the blockage[1,2]. A phased array antenna is the first choice for beam steering applications, but it is costly and difficult to design. The primary restriction on RF performance and cost is the feeding network of mm-wave phased arrays due to the extensive use of phase shifters, which results in a system that is extremely complex in terms of hardware, expensive, and power-inefficient, particularly for large antenna arrays[1]. Another way to control the direction of the antenna's radiation is mechanical beam steering. This method is cheaper, yet the antennas are usually bulkier than phased array antennas[3]. Reflect and transmit arrays for beam steering applications are becoming increasingly popular due to their low cost and ease of design while maintaining good RF performance[3]. A typical geometry of a reflectarray antenna has been shown in Fig. 1. Various methods are proposed by the researchers for tilting an antenna's beam using a reflect/transmit array based on mechanical/passive beam steering[4–11] and electronic/active beam steering[12–19]. The first can be realized electronically by incorporating active devices like PIN diodes and switches into single or multilayer periodic structures called metasurfaces, frequency-selective surfaces (FSS) or intelligent reflective surfaces (IRS). However, this approach requires expensive hardware with increased complexity at mm-wave frequency. The second way is to tilt the beam mechanically using actuators.

[1]Faculty of Electronics, Telecommunications, and Informatics, Gdansk University of Technology, 80-233 Gdansk, Poland. [2]Engineering Optimization and Modeling Center, Reykjavik University, 101 Reykjavik, Iceland. ✉email: koziel@ru.is

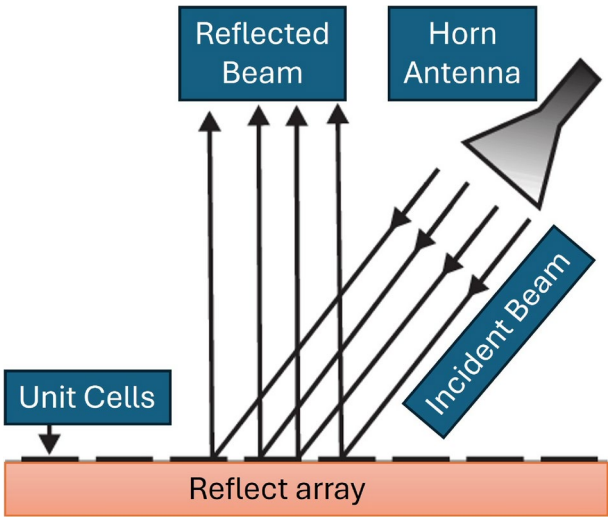

Fig. 1. Typical geometry of a reflectarray antenna.

This includes mechanical steering by rotating, tilting, or translating the feed source or the metasurface along an axis. However, these approaches are not practical when employed without any external mechanical control system.

To the best of the authors' knowledge, a high-gain beam-steerable dual-band MIMO antenna based on a passive conformal reflective metasurface for mm-wave 5G bands has not yet been reported in the available literature. Most of the research focuses on active beam steering using reconfigurable metasurfaces. Many metasurface based antenna designs have recently been reported in the literature for beam steering applications[4–23]. Metasurfaces have been extensively utilized to perform beam steering and polarization transformation. In[23], a non-orthogonal metasurface have been proposed for polarization transformation and have experimentally demonstrated the concept with nearly unity efficiency performances. The simulated and measured maximum efficiency reaches 99% and 97%, respectively for incident angle of up to 60ř. In[12], a transmit array antenna based on a phased array is presented. It uses phase shifters and switches to achieve a beam steering range of $+30^0$. Likewise, in[13] an active beam steerable metasurface lens antenna for mm-wave applications is presented. It uses a patch array as a source antenna to achieve a beam steering of up to 30^0 at 28 GHz. A dual-layer and dual-band shared-aperture metasurface antenna integrated with a horn antenna is presented in[24] for beam steering applications at 13 and 38 GHz. In another recent publication, a beam-tilting end-fire antenna based on a single-layer FSS is reported for 5G communications[5]. Beam steering from -23^0 to $+29^0$ was achieved by manually rotating the FSS with a maximum gain enhancement of 1 dB for the desired operating bands of 28 and 31 GHz. In[7], a beam steerable metasurface antenna is proposed by manually altering the feed antenna using a stepper motor and a control system when deployed. In[22], a metasurface based reflector is placed at the back of a two-port MIMO configuration. Its sole purpose is to improve the gain (a peak gain of 11.5 dB is attained) without enabling beam steering. In another research work[25], a high-gain dual circularly polarized reflector antenna fed by a circular horn antenna is proposed. This design exhibits high gain, excellent isolation, and effective dual circular polarization characteristics. However, the proposed reflector antenna structure is complex, bulky, and inconvenient for practical applications. In[26], a beam steerable metasurface antenna is presented and achieved beam steering electronically from -32^0 to $+30^0$ without changing the position of the antenna and the metasurface. The majority of transmit/reflect array metasurfaces presented in the state-of-the-art sources used horn antennas as a feeding source, which is not only expensive but also has a complex and bulky construction that is difficult to manufacture and integrate. There is a significant continuing research effort to design high-gain and cost-effective antenna systems for beam-steering applications. The challenge is to combine the key features such as low cost, high gain, beam steering, and multiband operation in a single antenna system. Compared to conventional reflectarray antennas, the proposed conformal reflective metasurface used a planar MIMO antenna to provide better installation flexibility while requiring less manufacturing complexity.

This work proposes a low-cost dual-band conformal reflective metasurface driven by a five-element MIMO antenna for high-gain beam steering applications in the mm-wave frequency bands. We propose an innovative and modest technique for passive beam steering, covering the ś40^0 range without using any active component or mechanical actuators. The proposed concept employs a passive conformal reflective metasurface for beam steering, so it is also cost-effective and lightweight. As a result, it may be deployed on a variety of sites, including rooftops, walls, and lamp posts, as well as unmanned Aerial Vehicles (UAVs) like drones to extend coverage. The conformal reflective metasurface can dynamically control the reflection across a wide range of angles. Furthermore, the suggested antenna is simple and compact, offering significantly higher gain than current designs. The major contributions of this study have been highlighted below:

This research is the first of its kind in demonstrating how a conformal passive reflective metasurface can be used for beam steering as well as gain enhancement. A novel and simple dual-band passive beam steering

antenna based on a conformal reflective metasurface has been designed and demonstrated to allow for $\$40^0$ coverage with a consistent high gain across the scanning range.
The suggested beam-steering antenna system is distinguished by its compact size, low profile, and low fabrication cost, as it employs only one single-layer passive metasurface and a planar MIMO antenna. As a proof-of-concept, a prototype of a reflective metasurface fed by a dual-band MIMO was fabricated and measured.
The feeding MIMO antenna is not only compact but also offers a wideband response at the desired 5G mm-wave bands. The critical features of the reflective metasurface include single-layer miniatured unit cells with a symmetric design, which makes it polarization insensitive and also suitable for conformal multiband applications.
The proof-of-concept experiment was conducted without using any active elements, switches, or control mechanisms normally used in beam scanning techniques. To demonstrate the concept while minimizing complexity and cost, we validated our approach by manually activating the specific antenna element for measurements.
This article is organized as follows. Section II discusses the general design considerations and simulation model of a reflective metasurface. Fabrication and measurements are provided in Section III to validate the design, followed by the concluding remarks in Section IV.

Proposed antenna design

This section outlines the structure and design of the proposed beam-steerable conformal reflective metasurface fed by a MIMO antenna. In sub-section I, the design and analysis of the proposed conformal metasurface unit cell will be presented. A single-element patch antenna, along with the five-element MIMO designed based on the single-element patch antenna is presented in sub-section II. In sub-section III, the complete prototype of the beam steerable dual-band MIMO antenna and the design of a 3D-printed holder to integrate conformal reflective metasurface and MIMO are presented.

Conformal reflective metasurface design

The design evolution and the geometrical parameters of the dual-band reflective metasurface unit cell are shown in Fig. 2. It consists of a single substrate layer and single metal layers on top of the substrate. The design of the proposed unit cell consists of an outer square loop of length L_1, an inner circular ring of radius R, and a cross dipole of length L_3. It is apparent from the step-wise response of the proposed unit cell that the outer square loop mainly determines the lower reflection band, while the upper reflection band at 38 GHz is primarily controlled by the inner circular ring. The used substrate is Arlon AD 250 with a dielectric constant of 2.5, a loss tangent of 0.0015, and a thickness of 0.76 mm to make it conformal. CST Microwave Studio is used to analyze

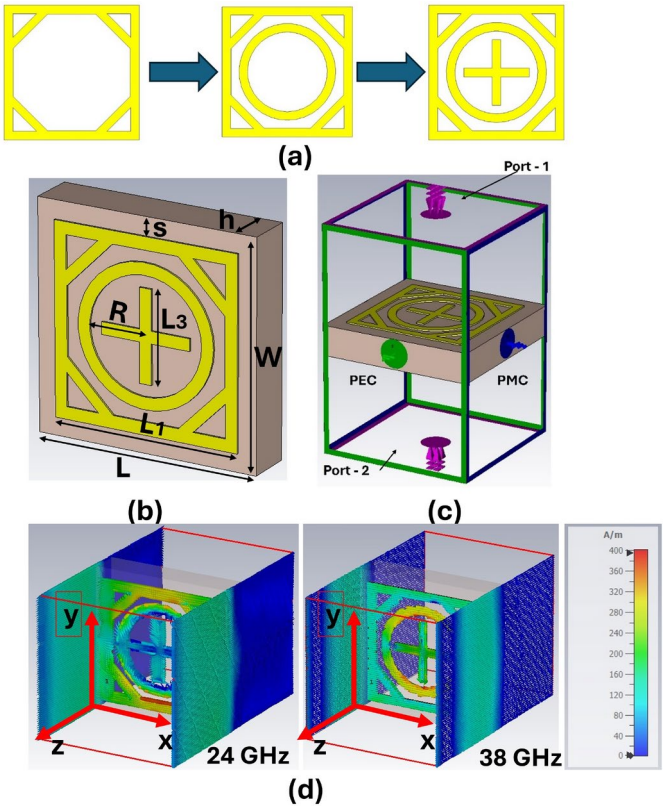

Fig. 2. Structure of proposed reflective metasurface unit cell: (**a**) design evolution, (**b**) geometrical parameters, (**c**) simulation model with boundary conditions, (**d**) surface current distribution.

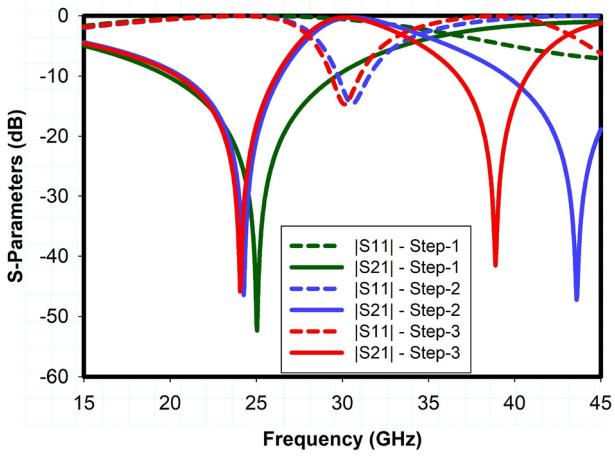

Fig. 3. Reflection and transmission coefficients of the unit cell.

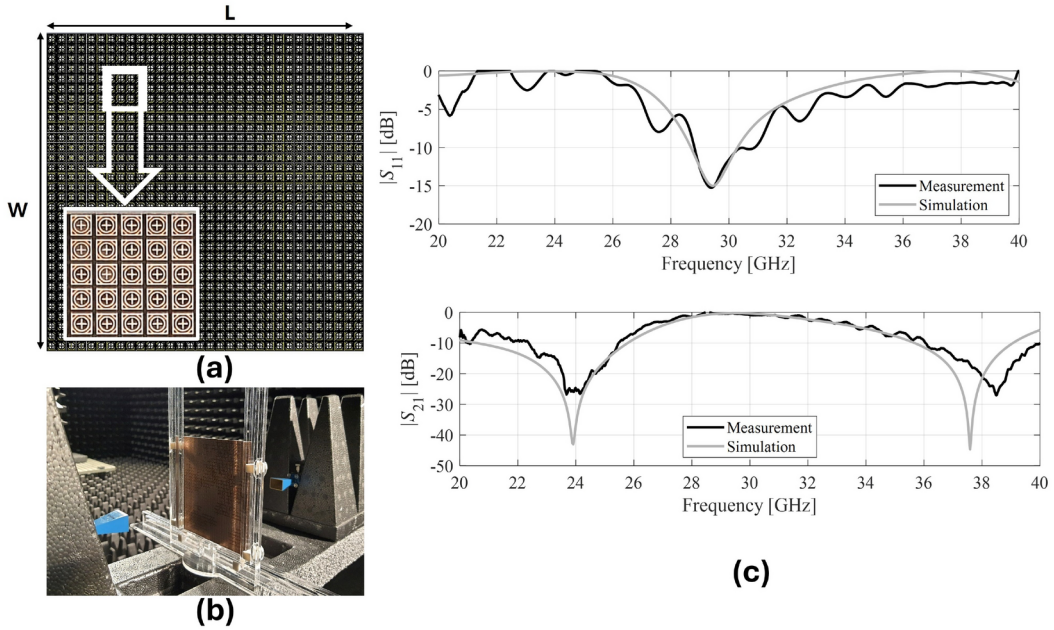

Fig. 4. (**a**) Prototype of 32 × 32 unit cells reflective metasurface, (**b**) measurement setup, (**c**) simulated and measured S-parameters response.

and optimize each parameter of the proposed metasurface. The unit cell boundary conditions are adopted to simulate the response of unit cells as shown in Fig. 2c. The detailed parametric analysis of the proposed reflective metasurface design is conducted and discussed in[27]. The transmission and reflection coefficients |*S*21| and |*S*11| of the proposed unit cell are presented in Fig. 3. It shows the dual reflection bands at 24 GHz and 38 GHz bands. Figure 2d exhibits the surface current distributions at 24 GHz and 38 GHz to facilitate understanding of the physical insights into the proposed unit cell structure. The surface current density is higher at the outer square ring of the unit cell at 24 GHz. On the other hand, a higher current density appears around the inner circular ring as well as on the cross dipole, which shows that the outer square ring is responsible for the operation in the lower frequency band, whereas the inner circular ring corresponds to the upper resonant frequency.

A 32 x 32 unit cell array with a total footprint of 118 × 118 mm² was successfully designed and simulated using CST MWS. The distance between the unit cells was optimized to achieve the desired response. The reflection (|S11|) and transmission (|S21|) coefficients of the reflective metasurface were measured in an anechoic chamber, as depicted in Fig. 4b. The measurement setup involved two Ka-band WR-28 standard gain horn antennas for transmitting and receiving the incident and reflected waves. The proposed metasurface was positioned between the horn antennas at 0.5 m, ensuring it was in the far-field region, as shown in Fig. 4b. The simulated and measured transmission and reflection coefficients of the reflective metasurface were compared and are presented in Fig. 4c. The single layer metasurface demonstrated two reflection bands, ranging from 19.5 to 26.2 GHz and

37.1–41.8 GHz, with fractional bandwidths of 27% and 12.5%, respectively. The measured results showed good stability and consistency with the simulated data. A conformal 32 *times* 32 array of unit cells was designed and simulated to further validate its performance under bending conditions, as illustrated in Fig. 5a. The behavior of the proposed metasurface was analyzed at different bending angles, as depicted in Fig. 5b. The transmission (|S21|) and reflection (|S11|) responses at these bending angles were compared with those of the flat metasurface (angle = 0ř), as shown in Fig. 5c. The overall transmission and reflection response of the proposed conformal reflective metasurface demonstrates remarkable stability, exhibiting only a minor impact from variations in bending "Angle" when compared to conventional flat metasurface. This characteristic validates its suitability for applications that require conformal surfaces, where flexibility and adaptability to varying geometries are essential.

As the bending angle increases, the effective area of the metasurface is influenced by the curvature introduced by the bending. This change in geometry leads to an increase in the capacitive coupling between the unit cells of the metasurface. This increase in capacitive coupling directly correlates with a slight shift in the resonant frequency of the metasurface as described by the Eq. (1). Specifically, as the bending angle approaches 60ř, the resonant frequency experiences a minor downward shift, indicating that the metasurface can adapt its operational frequency without significant degradation in performance.

$$f = 1/(2\pi\sqrt{(LC)}) \tag{1}$$

MIMO antenna design

A single-element microstrip patch antenna is designed on the Arlon AD 250 substrate resonating at dual mm-wave 5G bands (24 and 38 GHz). Figure 6a illustrates the step-by-step design evolution of the proposed feeding antenna. The complete simulation model of a single-element patch antenna, including the SMA connector, is shown in Fig. 6b. Three circular slots are symmetrically cut on the outer edges of the patch to achieve the desired dual-band response. Further, two rectangular slits are designed to improve the dual-band impedance matching with the input 50-ohm transmission line. The substrate used is Arlon AD 250 of a thickness h = 0.76 mm, a dielectric constant of 2.5, and a dissipation factor of 0.0015. The surface current distribution gives a detailed overview of the dual-band behavior of the proposed design at 24 and 38 GHz as shown in Fig. 6c. The surface current has a higher density at the circular slits at the outer edges of the square patch therefore, the circular slits on the outer edges of the patch mainly correspond to the lower frequency band at 24 GHz. On the other hand, a higher current density appears around the inner two rectangular slits as well as on the whole patch which shows that the two rectangular slits along the transmission line correspond to the upper resonant frequency band at 38 GHz as illustrated in Fig. 6c. The S-parameters (|S11|) response and E-plane radiation pattern of the proposed

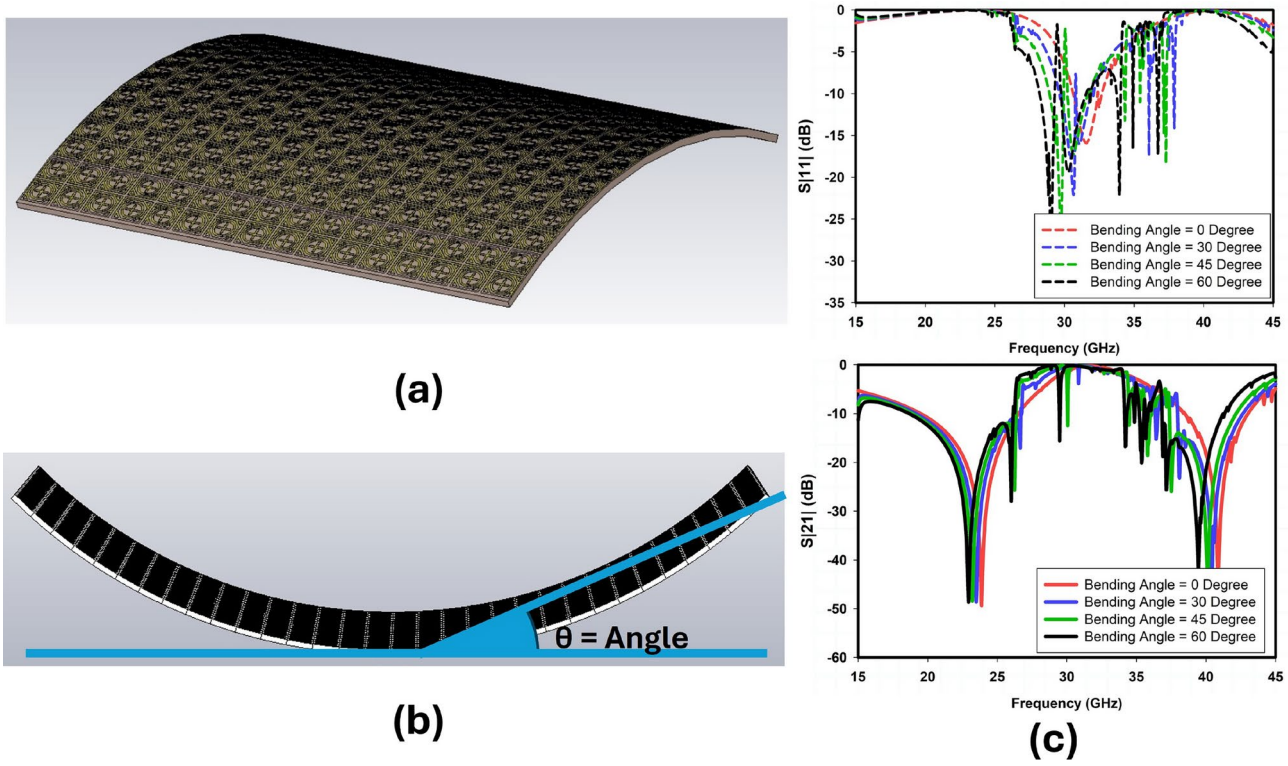

Fig. 5. (**a**) Simulation model of conformal reflective metasurface, (**b**) side view, (**c**) simulated S-parameters response.

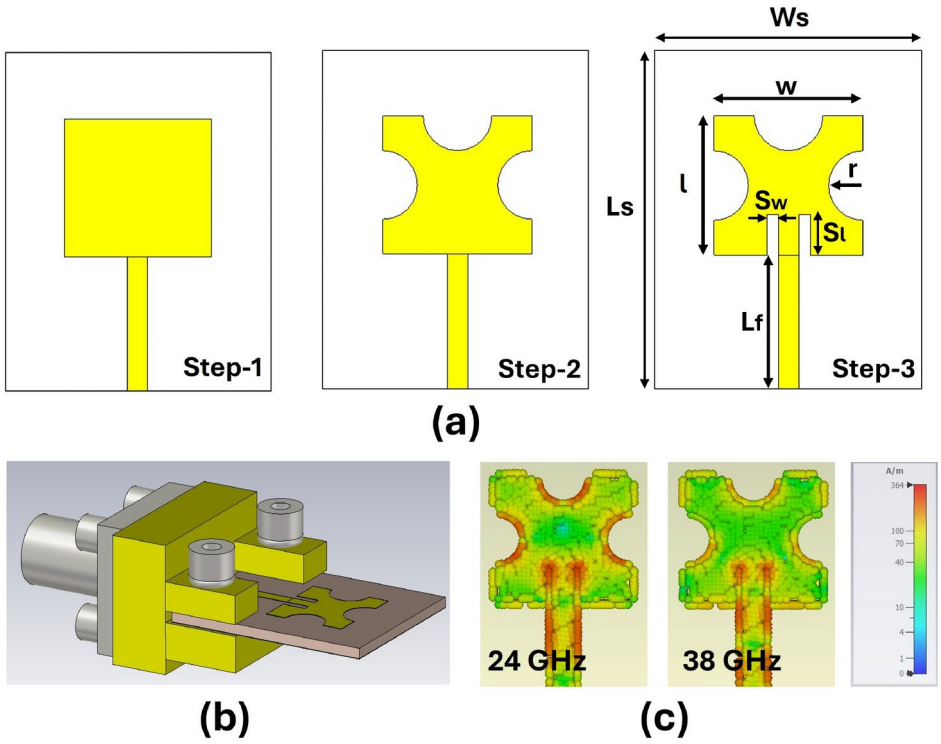

Fig. 6. Single element patch antenna: (**a**) design evolution, (**b**) final simulation model with the SMA connector, (**c**) surface current distribution.

single-element antenna are presented in Fig. 7a,b, respectively, which demonstrate the dual-band response of the MIMO antenna.

The structure of the proposed five-element MIMO, which is designed based on the single-element antenna is shown in Fig. 8. The coupling between the elements is optimized based on the spacing between the elements. Following the analysis, a center-to-center inter-element spacing of 15 mm is selected to arrange the MIMO elements linearly in a row with a total footprint of 70×12 mm^2. The mutual coupling between the antenna elements does not exceed -22 dB. The gain of each antenna element in this configuration is 5.4 dB and 7.2 dB at 24 and 38 GHz, respectively. The simulated outcomes of the proposed MIMO in terms of reflection coefficient $|S11|$ and envelop correlation coefficient (ECC) are shown in Fig. 9a,b, respectively. The ECC is an important parameter to determine the isolation or correlation between the various communication channels in MIMO antenna systems. The ECC value should be zero for complete isolation between the MIMO elements, however, for practical applications, a value lower than 0.5 is sufficient to offer high diversity performance. ECC's lower (close to zero) value indicates that the MIMO channels will be largely independent when employing the suggested MIMO antenna array structure. Table 1 summarizes the dimensions of the design parameters of the proposed MIMO antenna and metasurface unit cell.

Complete model and working principle of reflective metasurface antenna

The geometrical configuration of the proposed beam steerable reflective metasurface fed by the MIMO antenna is shown in Fig. 10a. The proposed beam steering antenna consists of three main parts: a large 32×32 unit cells conformal dual-band reflective metasurface as shown in Fig. 4 and discussed in Section 2.1, a planar 5-element MIMO antenna as shown in Fig. 8 and discussed in Section 2.2, and a 3D printed holder to integrate the conformal reflective metasurface with the MIMO antenna as shown in Fig. 10b.

The working principle of our proposed design is illustrated in Fig. 10c and is based on the concept of angle reciprocity in passive reflective metasurface. Figure 10d demonstrates the angle reciprocity response of our proposed reflective metasurface across a range of incidence angles from 0ř to 60ř at frequencies of 24 GHz and 38 GHz. The results indicate that our reflective metasurface maintains a wide and stable angle reciprocity up to a 60ř angle of incidence. In our design, the bending angle () and the position of the conformal reflective metasurface are fixed, with only one parameter (d_x) controlling the direction of the beam by changing the angle of incidence, which is equal to the angle of reflection. We have two options to implement this scenario for beam steering. First, we can use a single feed antenna element to achieve two-dimensional beam steering by manually moving the feed antenna under the conformal reflective metasurface, as shown in Fig. 10c. Alternatively, we can use multiple feed antennas placed at different positions and manually activate the specific antenna elements for beam steering as shown in Fig. 10a. The necessary feed displacement can be achieved using a single stepper motor, or we can employ an RF switch to control beam switching. This approach offers a simpler implementation and lower power consumption compared to phased arrays or reflectarrays that require numerous active elements

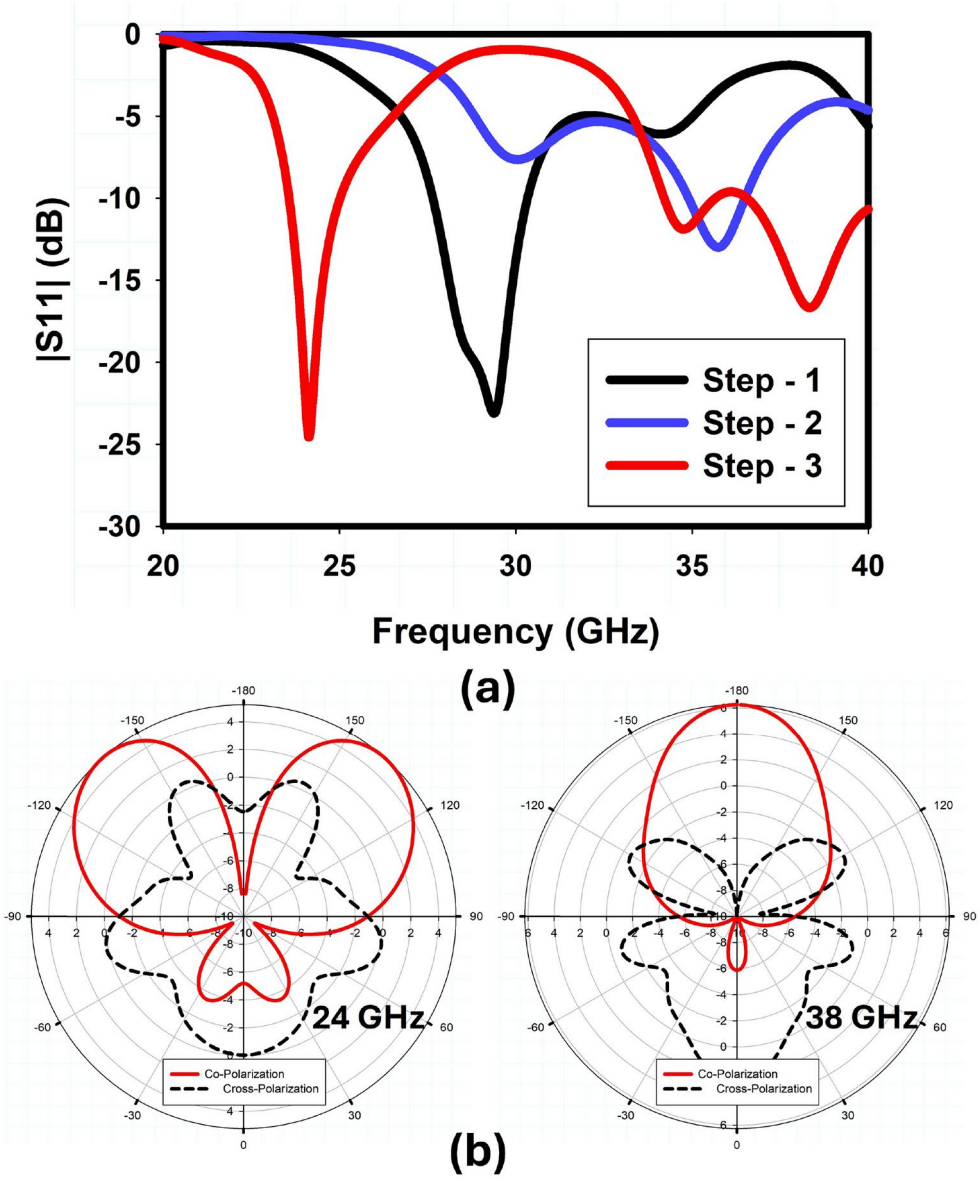

Fig. 7. Simulated results of proposed dual-band single-element patch antenna; (**a**) S-parameter coefficient (S|11|), (**b**) E-plane (phi = 0) radiation Pattern at 24 38 GHz.

for each unit cell of the apertures. Unlike existing beam steering strategies, our proposed method is not only cost-effective but also enhances the directivity and gain of the source antenna. The proposed conformal reflective metasurface based MIMO antenna setup provides a significant gain enhancement of up to 8 dB when compared to the source antenna. At the same time, a maximum beam steering range from -4^o to 4^o is achieved by adjusting the position (d_x) from -30 to 30 mm without much reduction in gain at the resonant frequencies of 24 and 38 GHz.

The gap between the conformal reflective metasurface and the feed antenna is a crucial design parameter that must be tuned to maximize the gain enhancement and reduce the side lobe levels. On the one hand, extending the gap will result in the energy leak from the edges of the conformal reflective metasurface, which will degrade the antenna's overall performance as well as increase the overall profile of the complete antenna design. However, if the gap is too short, the metasurface's loading effect on the feed antenna will be severe. This can adversely impact the radiation properties of the reflected beam and, in turn, the performance of the entire antenna model. The second major factor influencing the radiation pattern and the range of beam steering is the bending angle of the reflective metasurface allocated on top of the feed antenna. An extensive set of simulations was conducted to determine the optimum values for the bending angle and the gap between the reflective metasurface and feed antenna. As a result, the final prototype features an optimal gap of 30 mm between the MIMO antenna and the conformal reflective metasurface and a bending angle of 75 degrees. Figure 11a,b show the simulated reflection coefficient |S11| and port isolation characteristics, respectively, of the entire model of the proposed

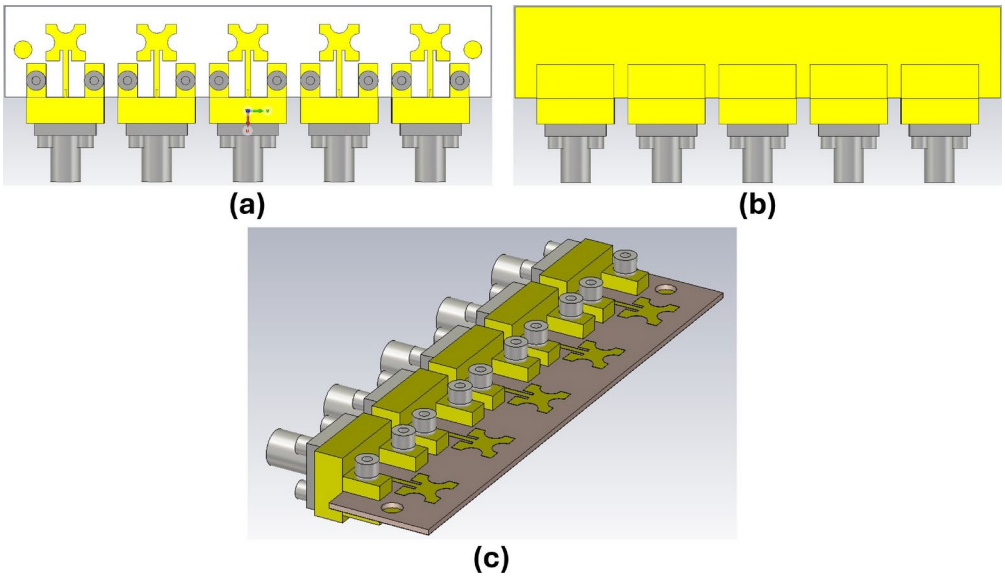

Fig. 8. Design configuration of proposed 5-element MIMO antenna with SMA connectors: (**a**) top view, (**b**) bottom view, (**c**) perspective view.

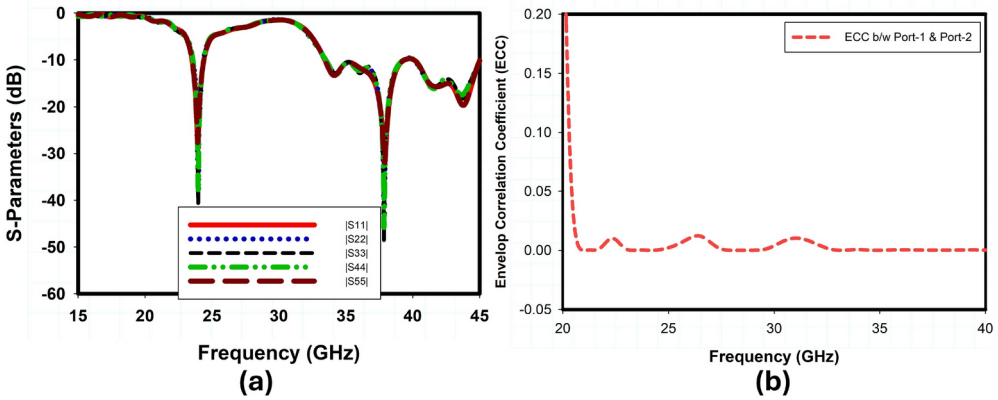

Fig. 9. Simulated results of the proposed dual-band MIMO antenna, (**a**) reflection coefficient |S11|, (**b**) envelop correlation coefficient (ECC).

Parameters	Values (mm)	Parameters	Values (mm)
L_s	15	W_s	12
r	1.5	h	0.76
S_l	1.75	S_w	0.5
L_f	9	W_f	0.9
l	6.5	w	6
L_1	3.1	R	1.15
s	0.2	d	15
L	118	W	118

Table 1. Optimized values of the reflective metasurface unit cell and the MIMO antenna.

beam steerable conformal reflective metasurface antenna. The ports of the MIMO antenna are associated with the five switched beam positions. These beams are individually steered by activating the appropriate port to excite the MIMO elements. Since the five elements of MIMO are at distinct spatial locations concerning the conformal reflective metasurface, the radiated beams from each antenna are steered in different directions, as

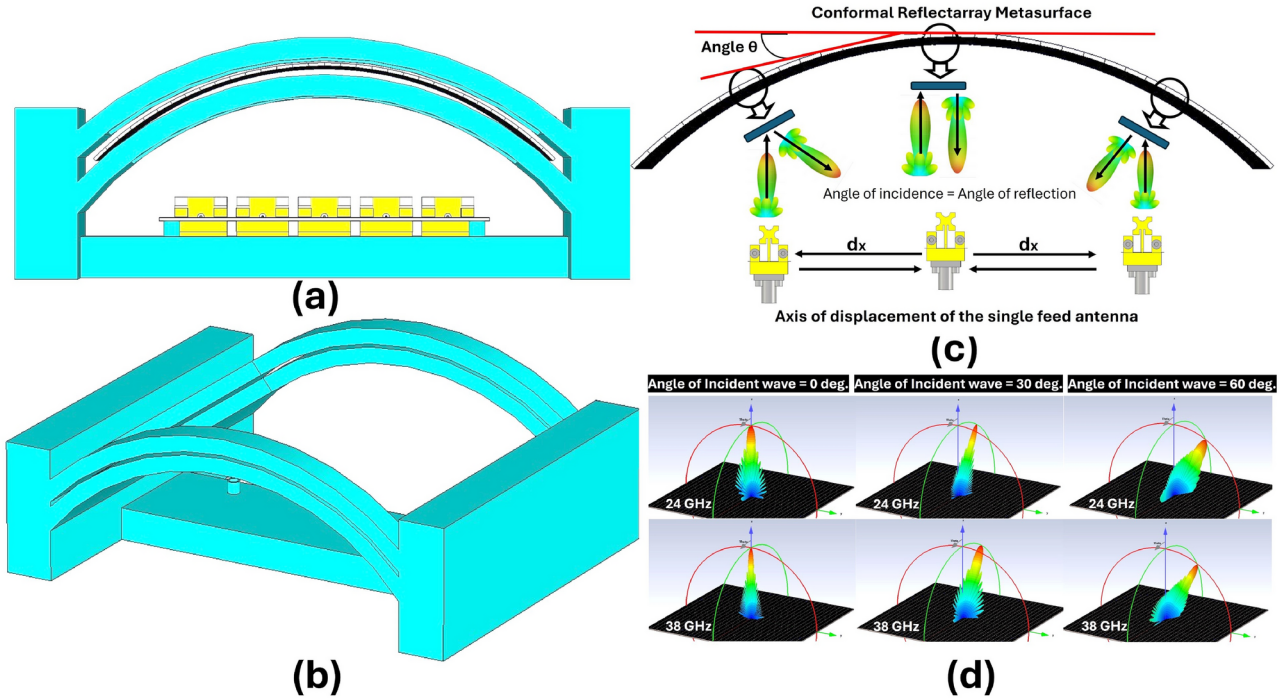

Fig. 10. Proposed beam steerable reflective metasurface antenna: (**a**) model of the 3D-printed holder, (**b**) complete model, (**c**) Working principle, (**d**) angle reciprocity for different angles of incident wave.

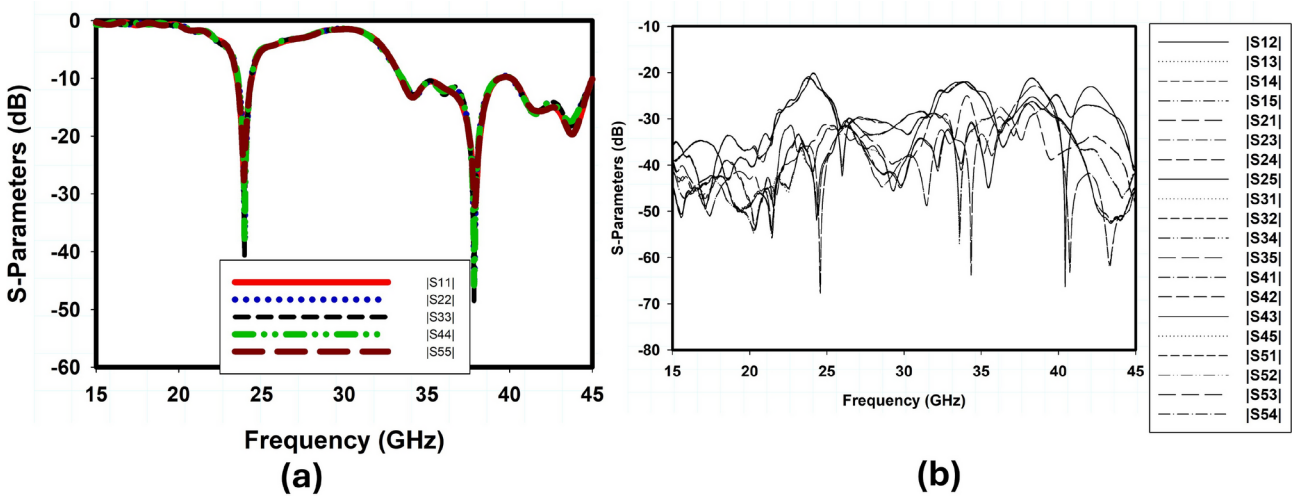

Fig. 11. Proposed reflective metasurface based MIMO antenna: (**a**) reflection coefficients, (**b**) mutual coupling between the MIMO antenna elements.

illustrated in Figs. 12 and 13. The performance evaluation parameters of the proposed model are summarized in Table 2.

Experimental validation and benchmarking

To experimentally validate the proposed beam-steerable antenna design, a complete prototype has been manufactured and assembled. The structure comprises a 118.6 × 118.6 mm^2 single-layer conformal reflective metasurface for beam steering, a five-port MIMO as a source antenna, and a 3D-printed holder to integrate the MIMO and conformal metasurface. The fabricated and assembled prototype of the reflective metasurface fed by a MIMO antenna is shown in Fig. 14a. The first and the most critical part of the proposed design is the dual-band conformal reflective metasurface fabricated using a thin flexible substrate material to make it conformal. The second major part of the complete prototype is the dual-band source MIMO antenna. Both parts were fabricated and measured separately to analyse their performance individually. A 3D-printed holder is designed in CST

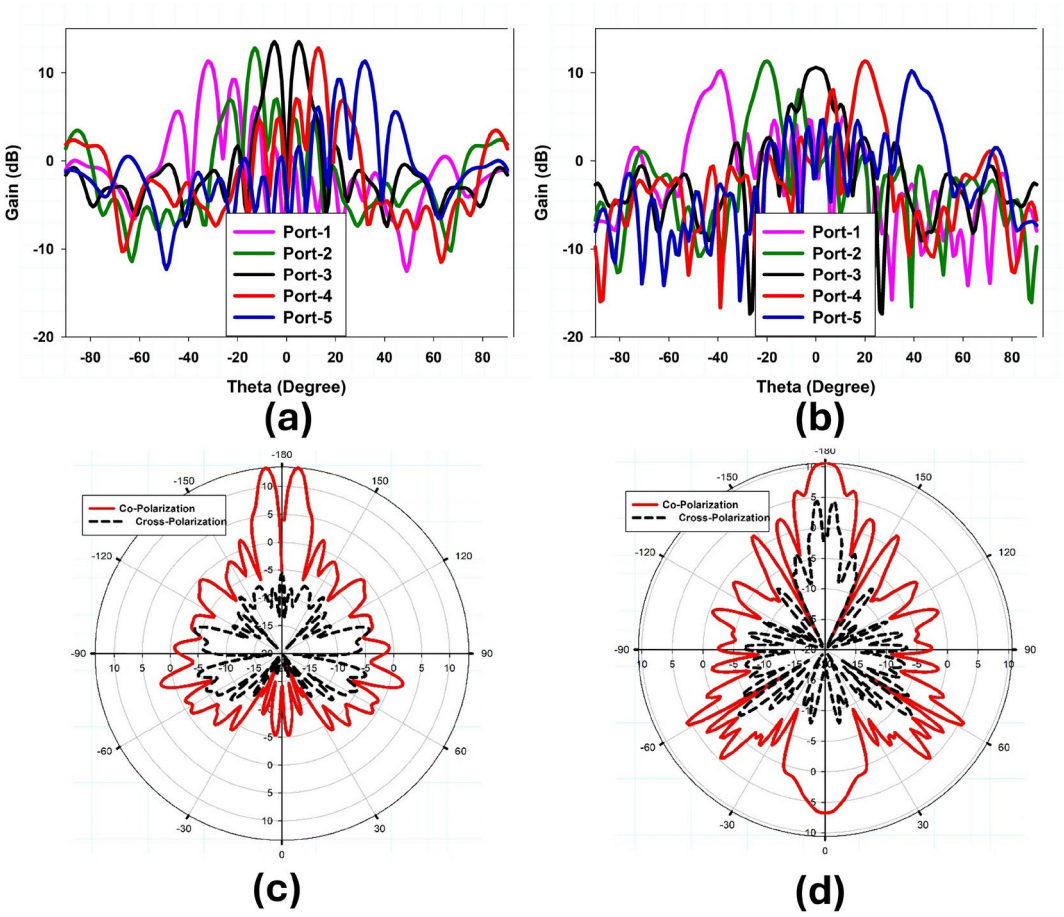

Fig. 12. E-plane (phi = 0) rectangular plots of the radiation pattern of the proposed reflective metasurface based antenna for different ports of MIMO, (**a**) 24 GHz, (**b**) 38 GHz, (**c**) Port-3 (24 GHz), (**d**) Port-3 (38 GHz).

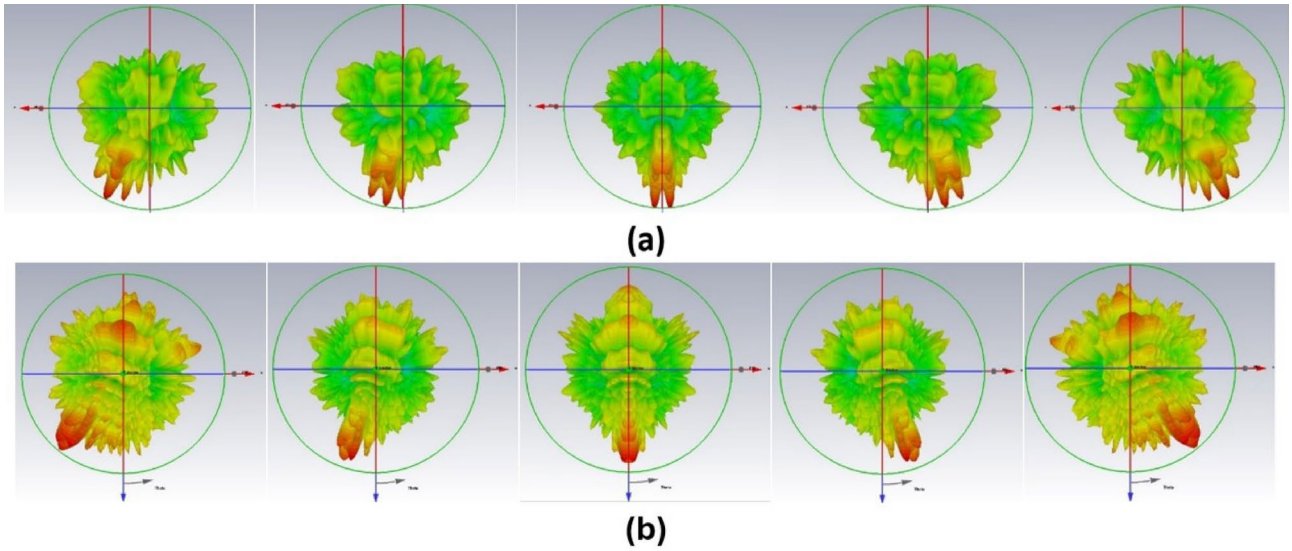

Fig. 13. 3D Polar plots of the proposed beam steerable antenna. From left to right: Port-1 to Port-5 of the MIMO structure: (**a**) 24 GHz, (**b**) 38 GHz.

Antenna/port	Front-back-ratio (dB)		Side lobe level (dB)		Gain (dB)		Rad. efficiency (%)	
	24 GHz	38 GHz	24 GHz	38 GHz	24 GHz	38 GHz	24 GHz	38 GHz
1	15.3	19.8	−5.1	−5.2	10.6	10.4	83	88
2	26.2	17.2	−5.8	−3.2	12.5	13.6	79	86
3	18.7	13.6	−11.1	−5.8	13	13.85	79	86
4	26.2	17.2	−5.8	−3.2	12.45	13.6	79	86
5	15.3	19.8	−5.1	−5.2	10.5	10.4	84	86

Table 2. Performance evaluation Parameters of proposed reflective metasurface based MIMO antenna.

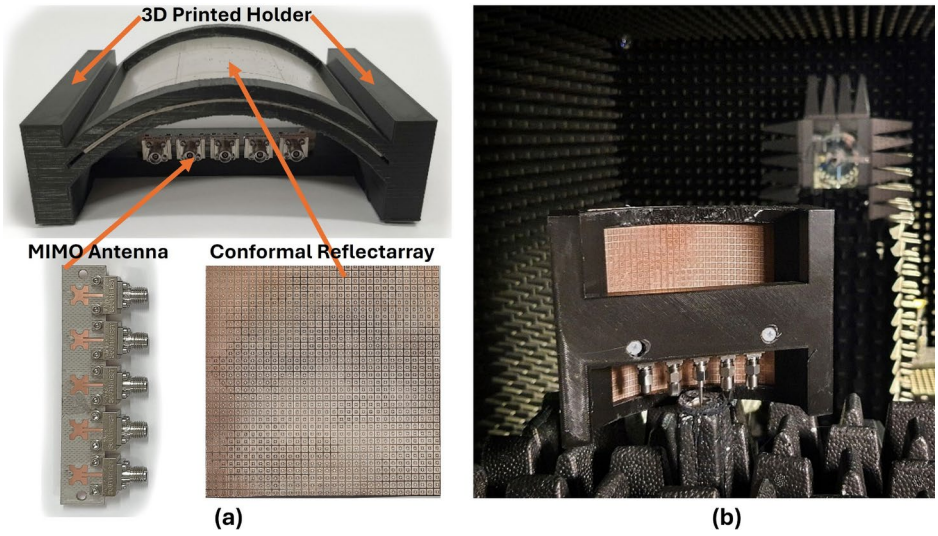

Fig. 14. Experimental validation of the proposed beam-steerable antenna: (**a**) fabricated and assembled prototype, (**b**) measurement setup in an anechoic chamber.

MWS and realized using the in-house 3D printing facility to integrate the conformal reflective metasurface and the feed source MIMO antenna. Polylactic acid (PLA) material with a low dielectric constant of 2.5 is used to print the holder to minimize its effect on the performance of the complete prototype. To validate the simulated outcomes, the proposed beam-steerable antenna is measured in an anechoic chamber. As seen in Fig. 14b, the measuring setup comprises a receiver standard gain horn antenna positioned in the far field of the antenna under test (AUT). The normalized far-field E-plane radiation patterns from Ports 1 to 5 of the MIMO antenna with a conformal reflective metasurface at 24 and 38 GHz are plotted in Fig. 15. First, Port 1 of the MIMO enabled to radiate the beam at 40^0. Likewise, switching the ports of MIMO from Port 1 to Port 5 steered the beams from 40^0 to $+40^0$ as depicted in Fig. 15a–e at 24 GHz, and in Fig. 15f–j at 38 GHz. The simulated and measured radiation patterns are consistent and validate the proposed beam steering approach. For the 24 GHz band, the measured gain is 13.1 dB and sidelobe levels are better than -11 dB. For the 38 GHz band, the measured gain is 14.2 dB and the sidelobe levels are less than -5 dB. A comparison of measured and simulated reflection coefficients $|S11|$ at Ports 1, 2, and 3 of the proposed conformal reflective metasurface fed by a MIMO antenna is plotted in Fig. 16a–c, respectively. The port isolation characteristics of the proposed antenna are presented in Fig. 16d, which shows the mutual coupling response of less than -20 dB for all ports. The measured results are indicative of the dual-band response of the proposed antenna at all ports with a satisfactory impedance matching at 24 and 38 GHz and -10 dB impedance bandwidths of 23.5–24.8 GHz, and 36.1–41.3 GHz, respectively, agreeing well with the simulations.

As indicated in comparison Table 3, the design presented in this work performs well and demonstrates the effectiveness of the proposed design strategy. To demonstrate the advantages of our strategy, we compared it with existing metasurface based beam steerable antennas recently reported in the literature. Table 3 compares the various major parameters of the beam steering antennas. The fundamental advantage of the proposed design approach over previously reported structures is its low cost and low profile because it uses a planar MIMO antenna as feed instead of horn antennas utilized by most reported studies presented in Table 3. However, the maximum gain of our design is lower than those reported in[9,11,17,18,29], since they used high-gain horn antennas as source antenna, unlike low-cost planar patch antennas. Secondly, the proposed design does not use any active component in the reflective metasurface to steer the antenna beam from 40^0 to $+40^0$ in contrast to[12,13,16–18]. Our reflective metasurface design exhibits low-cost, compact, low-profile, and low-complexity features, allowing for

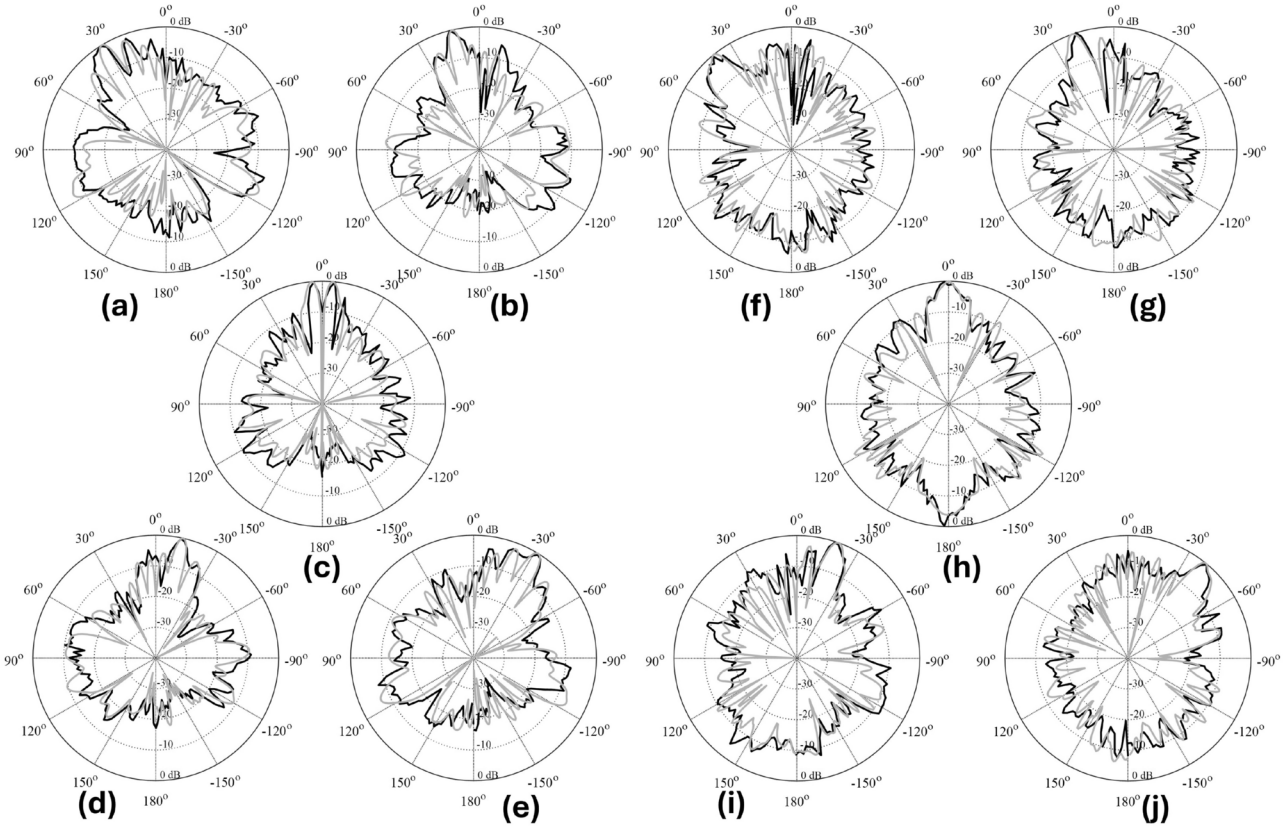

Fig. 15. Measured versus simulated normalized E-plane (phi = 0) radiation patterns of the proposed antenna (Ports 1 through 5 from (**a**)–(**e**) at 24 GHz and from (**f**) to (**j**) at 38 GHz.

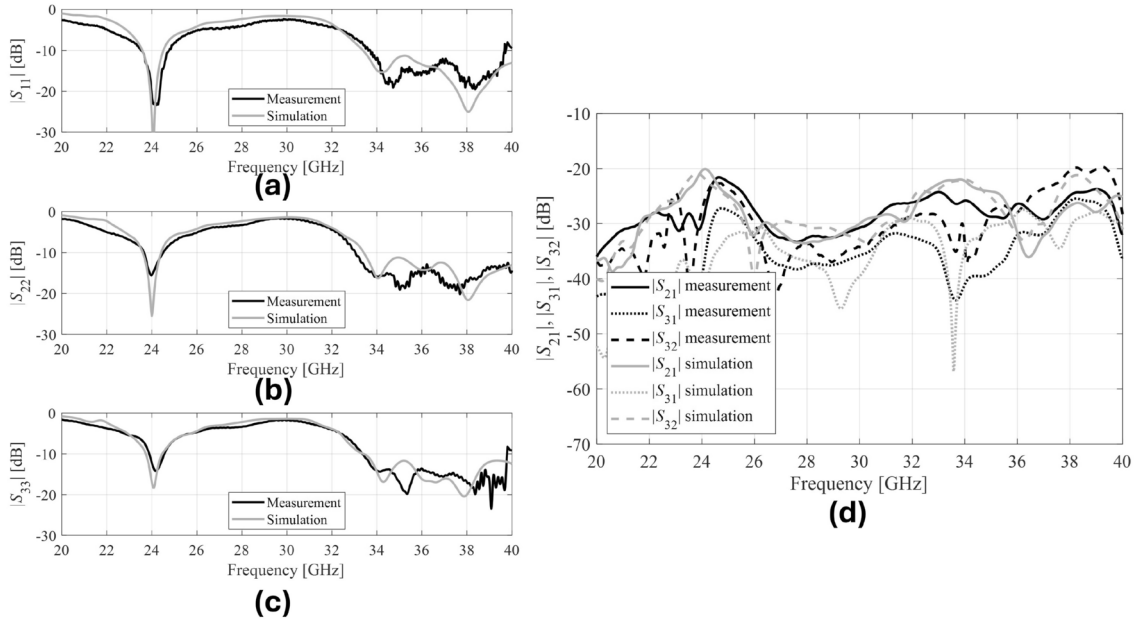

Fig. 16. Measured and simulated S-parameters of the proposed antenna (**a**) Port-1, (**b**) Port-2, (**c**) Port-3, (**d**) Port isolation characteristics.

Refs.	Array type	Feeding source	Frequency band (GHz)	Gain enhancement/peak gain (dBi)	Aperture size (mm^2)	Beam steering type	Beam steering range
[12]	Transmit	Patch array	10	11	216 × 72	Electronic (switches and phase shifters)	-30^0 to $+30^0$
[24]	Reflect	Horn antenna	13, 38	13.2	249 × 249	No	N/A
[13]	Transmit	Patch Array	28	19 Peak	75 × 75	Electronic (switches)	-30^0 to $+30^0$
[26]	Reflect	MIMO Antenna	240	10	36 × 40	Electronic (diodes)	-30^0 to $+30^0$
[5]	Reflect	Yagi-Uda Antenna	28, 31	1	130 × 90	Manually (rotating the FSS)	-23^0 to $+29^0$
[16]	Reflect/Transmit	Horn Antenna	4.9	19.4 Peak	360 × 360	Electronic (diodes)	-50^0 to $+50^0$
[28]	Reflect	MIMO Antenna	30	2	22 × 22	No	N/A
[6]	Reflect	MIMO Antenna	28	3.5	N/A	Mechanically through metallic walls	0^0 to $+30^0$
[7]	Reflect	Horn Antenna	5.8, 10	14.4 Peak	133 x 135	Manually using a stepper motor	-40^0 to $+40^0$
[8]	Transmit	Horn Antenna	14	17.8 Peak	119 × 121	Manually by rotation of the lens	-50^0 to $+50^0$
[9]	Transmit	Horn Antenna	20, 30	22.5 Peak	N/A	Manual rotation of the Transmit array	-40^0 to $+40^0$
[29]	Transmit	Horn Antenna	19, 29	25 Peak	N/A	Electronic	-33^0 to $+33^0$
[18]	Reflect	Horn Antenna	5	17.9 Peak	400 × 360	Electronically through pin diodes	-50^0 to $+50^0$
[19]	Transmit	Patch Antenna	5	10.8 Peak	150 x 150	Electronically through pin diodes	-22^0 to $+22^0$
[17]	Reflect	Horn Antenna	12.5	17 Peak	N/A	Electronically through diodes	-60^0 to $+60^0$
[30]	Reflect	Horn Antenna	28	9.7 Peak	279 x 279	NO	N/A
[10]	Transmit	Cavity Antenna	20, 30	5	80 × 80	Manual displacement of transmit array and feed	0^0 to $+24^0$
[11]	Transmit	Horn Antenna	20, 30	24 Peak	N/A	Manual displacement of feed	0^0 to $+50^0$
This Work	Reflect	MIMO Antenna	24, 38	14.2 Peak	N/A	Manually activating the ports of MIMO	-40^0 to $+40^0$

Table 3. Comparison of the proposed design with state-of-the-art structures reported in recent literature.

beam steering spanning ś40^0 with utilizing any control setup for manual displacement of metasurface to achieve beam tilting as reported in[7–10].

Conclusion

A low-cost high-gain beam steerable antenna design comprising a conformal passive reflective metasurface and feed source MIMO antenna is proposed and validated experimentally for passive beam steering applications at the mm-wave 5G bands. In contrast to traditional electronic and mechanical beam steering methods, the suggested beam steerable antenna design uses a simple approach to achieve ś40ř beam steering using a conformal passive reflective metasurface fed by a five-port planar MIMO antenna. The beam steering range can be further extended using the proposed method by increasing the number of MIMO elements. To experimentally validate the proposed design approach, a complete prototype was manufactured, assembled, and characterized. The experimental results demonstrated that the proposed passive conformal reflective metasurface design allows for a beam steering range of ś40^0 and maintains a satisfactory realized gain without using any active component, including diodes, switches, and phase shifters or mechanical control system to steer the beam. Geometrical simplicity and low fabrication cost make the antenna a promising candidate for low-cost beam steering applications for the 5G mm-wave range.

Data availibility

The datasets used and/or analysed during the current study available from the corresponding author on reasonable request.

Received: 5 July 2024; Accepted: 7 October 2024
Published online: 15 October 2024

References

1. Wang, J., Cao, Y., Che, W. & Xue, Q. Wide-angle beam-scanning millimeter-wave antenna array using phase-controlled beam-steerable elements. *IEEE Trans. Antennas Propagat.* **72**, 3730–3735. https://doi.org/10.1109/TAP.2024.3361510 (2024).
2. Baba, A. A., Hashmi, R. M., Attygalle, M., Esselle, K. P. & Borg, D. Ultrawideband beam steering at mm-wave frequency with planar dielectric phase transformers. *IEEE Trans. Antennas Propagat.* **70**, 1719–1728. https://doi.org/10.1109/TAP.2021.3111637 (2022).
3. Joy, J. A. et al. Modern reflectarray antennas: A review of the design, state-of-the-art, and research challenges. *IEEE Access* **12**, 46717–46740. https://doi.org/10.1109/ACCESS.2024.3380358 (2024).
4. Alwahishi, R., Ali, M. M. M., Elzwawi, G. H. & Denidni, T. A. Beam-switching antenna using reconfigurable intelligent frequency selective surfaces for internet of things applications. *IEEE Internet Things J.* **11**, 4152–4162. https://doi.org/10.1109/JIOT.2023.3298908 (2024).

5. Mantash, M., Kesavan, A. & Denidni, T. A. Beam-tilting endfire antenna using a single-layer FSS for 5G communication networks. *IEEE Antennas Wireless Propagat. Lett.* **17**, 29–33. https://doi.org/10.1109/LAWP.2017.2772222 (2018).
6. Alkaraki, S. & Gao, Y. Mm-wave low-cost 3D printed MIMO antennas with beam switching capabilities for 5G communication systems. *IEEE Access* **8**, 32531–32541. https://doi.org/10.1109/ACCESS.2020.2973087 (2020).
7. Gu, L., Yang, W., Xue, Q. & Che, W. A $\pm 45^{\circ}$ dual-polarized dual-beam series-fed metasurface antenna array with stable beam angle. *IEEE Trans. Antennas Propagat.* **69**, 8366–8375. https://doi.org/10.1109/TAP.2021.3083833 (2021).
8. Zeng, Q., Xue, Z., Ren, W. & Li, W. Dual-band beam-scanning antenna using rotatable planar phase gradient transmitarrays. *IEEE Trans. Antennas Propagat.* **68**, 5021–5026. https://doi.org/10.1109/TAP.2020.2963929 (2020).
9. Wang, P., Ren, W., Zeng, Q., Xue, Z. & Li, W. Dual-band beam-scanning antenna at Ka-band by rotation of two transmitarrays. *IEEE Antennas Wireless Propagat. Lett.* **21**, 1792–1796. https://doi.org/10.1109/LAWP.2022.3180112 (2022).
10. Hasani, H., Silva, J. S., Capdevila, S., Garcia-Vigueras, M. & Mosig, J. R. Dual-band circularly polarized transmitarray antenna for satellite communications at (20, 30) GHz. *IEEE Trans. Antennas Propagat.* **67**, 5325–5333. https://doi.org/10.1109/TAP.2019.2912495 (2019).
11. Matos, S. A. et al. High gain dual-band beam-steering transmit array for satcom terminals at Ka-band. *IEEE Trans. Antennas Propagat.* **65**, 3528–3539. https://doi.org/10.1109/TAP.2017.2702658 (2017).
12. Xu, R. & Chen, Z. N. A compact beamsteering metasurface lens array antenna with low-cost phased array. *IEEE Trans. Antennas Propagat.* **69**, 1992–2002. https://doi.org/10.1109/TAP.2020.3026905 (2021).
13. Tiwari, S., Singh, A. K., Poddar, A. K., Rohde, U. L. & Dubey, A. Active beamsteerable digital metasurface lens antenna for millimeter-wave applications. *IEEE Antennas Wireless Propagat. Lett.* **22**, 2871–2875. https://doi.org/10.1109/LAWP.2023.3303135 (2023).
14. Duan, K. et al. Low-scattering and dual-polarized reconfigurable reflectarray antenna based on absorptive and active coding metasurfaces. *IEEE Trans. Antennas Propagat.* **72**, 2490–2501. https://doi.org/10.1109/TAP.2024.3356060 (2024).
15. Najafy, V. & Abbasi Arand, B. A novel dual-band beam scanning antenna based on slot active frequency-selective surfaces [antenna applications corner]. *IEEE Antennas Propagat. Magaz.* **63**, 94–143. https://doi.org/10.1109/MAP.2021.3069215 (2021).
16. Cao, X., Deng, C., Yin, Y., Hao, Y. & Sarabandi, K. 1-bit reconfigurable transmit- and reflect-array antenna using patch-ground-patch structure. *IEEE Antennas Wireless Propagat. Lett.* **23**, 434–438. https://doi.org/10.1109/LAWP.2023.3327442 (2024).
17. Xiang, B. J., Dai, X. & Luk, K. M. A wideband low-cost reconfigurable reflectarray antenna with 1-bit resolution. *IEEE Trans. Antennas Propagat.* **70**, 7439–7447. https://doi.org/10.1109/TAP.2022.3176868 (2022).
18. Li, G. et al. A simplified, double-layer and low-profile 1-bit reconfigurable reflectarray for 2-D space-time beam steering. *IEEE Antennas Wireless Propagat. Lett.* **23**, 658–662. https://doi.org/10.1109/LAWP.2023.3331721 (2024).
19. Ji, L. Y., Zhang, Z. Y. & Liu, N. W. A two-dimensional beam-steering partially reflective surface (PRS) antenna using a reconfigurable FSS structure. *IEEE Antennas Wireless Propagat. Lett.* **18**, 1076–1080. https://doi.org/10.1109/LAWP.2019.2907641 (2019).
20. Li, X., Sato, H., Fujikake, H. & Chen, Q. Development of two-dimensional steerable reflectarray with liquid crystal for reconfigurable intelligent surface applications. *IEEE Trans. Antennas Propagat.* **72**, 2108–2123. https://doi.org/10.1109/TAP.2024.3354054 (2024).
21. Yin, Y. et al. Design of a 2-bit dual-polarized reconfigurable reflectarray with high aperture efficiency. *IEEE Trans. Antennas Propagat.* **72**, 542–552. https://doi.org/10.1109/TAP.2023.3326951 (2024).
22. Sehrai, D. A. et al. Metasurface-based wideband MIMO antenna for 5G millimeter-wave systems. *IEEE Access* **9**, 125348–125357. https://doi.org/10.1109/ACCESS.2021.3110905 (2021).
23. Yuan, Y., Zhang, K., Wu, Q., Burokur, S. N. & Genevet, P. Reaching the efficiency limit of arbitrary polarization transformation with non-orthogonal metasurfaces. *Nat. Commun.*[SPACE]https://doi.org/10.1038/s41467-024-50560-1 (2024).
24. Liu, Y., Cheng, Y. J. & Fan, Y. A Dual-layer Ku/Ka Dual-Band Shared-Aperture Reflectarray Antenna Based on Structure-Reuse Technique. in *2021 IEEE International Symposium on Antennas and Propagation and North American Radio Science Meeting, APS/URSI 2021 - Proceedings*, 1925–1926, https://doi.org/10.1109/APS/URSI47566.2021.9704250 (Institute of Electrical and Electronics Engineers Inc., 2021).
25. Jiang, H. et al. High-gain dual circularly polarized antenna for air-to-ground wireless link. *Chin. J. Electron.* **31**, 555–561. https://doi.org/10.1049/cje.2021.00.257 (2022).
26. Das, P. Beam-steering of THz MIMO antenna using graphene-based intelligent reflective surface. *Optical Quant. Electron.*[SPACE]https://doi.org/10.1007/s11082-023-04996-2 (2023).
27. Malik, B. T., Khan, S. & Koziel, S. Design and implementation of multi-band reflectarray metasurface for 5G millimeter wave coverage enhancement. *Sci. Rep.*[SPACE]https://doi.org/10.1038/s41598-024-66330-4 (2024).
28. Shariff, B. G. et al. Design and measurement of a compact millimeter wave highly flexible MIMO antenna loaded with metamaterial reflective surface for wearable applications. *IEEE Access* **12**, 30066–30084. https://doi.org/10.1109/ACCESS.2024.3368394 (2024).
29. Pham, T. K., Guang, L., González-Ovejero, D. & Sauleau, R. Dual-band transmitarray with low scan loss for satcom applications. *IEEE Trans. Antennas Propagat.* **69**, 1775–1780. https://doi.org/10.1109/TAP.2020.3031410 (2021).
30. Tiwari, S., Singh, A. K. & Dubey, A. Additively manufactured dielectric reflectarray antenna for millimeter-wave satellite communication. *IEEE Antennas Wireless Propagat. Lett.* **23**, 1276–1280. https://doi.org/10.1109/LAWP.2024.3351891 (2024).

Acknowledgements

The authors would like to thank Dassault Systemes, France, for making CST Microwave Studio available. This work is partially supported by the Nobelium Joining Gdansk Tech Research Community DEC-17/2021/IDUB/I.1, and by Icelandic Research Fund Grant 2410297.

Author contributions

Conceptualization, B.T.M. (Bilal Tariq Malik); Data curation, S.K. (Slawomir Koziel) and B.T.M.; Formal analysis, B.T.M.; Funding acquisition, S.K; Visualization, B.T.M. and S.K.; Writing-original draft, B.T.M.; Writing-review and editing, S.K. and S.Kh. (Shahid Khan); Sofware and Resources, S.K; Supervision, S.K.

Declarations

Competing interests

The authors declare no competing interests.

Additional information

Correspondence and requests for materials should be addressed to S.K.

Reprints and permissions information is available at www.nature.com/reprints.